

中国激光

三腔复合光力系统的透射谱和四波混频现象研究

廖庆洪*, 邱海燕, 喻富, 肖敏

南昌大学电子信息工程系, 江西 南昌 330031

摘要 研究了三腔复合光力系统中探测场的透射系数和四波混频现象。结果表明:改变两个光学腔之间的耦合强度,可以使光力诱导透明现象发生显著变化。此外,在共振情况下,通过控制两个光学腔之间的耦合强度并改变机械振子的频率,可以对四波混频谱进行调制。通过双场探测手段,利用四波混频谱中的尖峰位置,实现了机械振子振动频率的精确测量。

关键词 量子光学; 复合光力系统; 透射谱; 四波混频; 光力诱导透明

中图分类号 O436 文献标志码

DOI: 10.3788/CJL221046

1 引言

腔光力学领域发展迅速^[1-2],该领域研究的电磁和机械系统可以实现对光力系统中光学响应的控制^[3-5]。光力系统由机械谐振器与光学腔耦合组成,提供了操纵机械谐振器和电磁场的平台,为光机械设备的潜在应用铺平了道路,例如声子激光器^[6]、传感^[7]、声子压缩^[8]、压缩光的实现^[9]等。此外,通过对腔施加强驱动可以增强有效光力耦合强度。当泵浦激光驱动腔至蓝边带时,在光力系统中可观察到量子纠缠^[10]、微波放大^[11]等现象。当泵浦激光驱动腔至红边带时,实验上获得了很多重要进展,例如基态冷却^[12]、量子态转化^[13]、光力诱导透明^[14-15]和四波混频^[16]等。其中,光力诱导透明与电磁诱导透明类似,主要是由干涉效应或者激发态中的暗态共振引起的。四波混频过程在不同光力系统中也得到了广泛的研究,例如强耦合光力系统中的模式分裂^[17]、相干机械驱动光力系统^[18]和双模腔光力系统^[19-20]等。

近年来,三腔光力系统引起了人们的广泛关注。Wang^[21]提出了一种在三腔光力系统不可分辨边带区域中将机械谐振器冷却至基态的方案。文献[22]研究了一种在三腔光力系统中实现量子限制方向放大器的方案。此外,研究者对复合腔光力系统中的非线性光学现象进行了深入的研究,如复合光子-分子腔光力系统中的光学双稳态和四波混频过程^[23]。本课题组研究了超导量子比特耦合微波腔和机械谐振器系统的探测场吸收特性^[24]。陈咏雷等^[25]研究了复合旋转光力系统的光学双稳态行为和四波混频现象。文献[26-27]分别

研究了复合腔光力系统中的双光子散射以及非旋转波近似效应的光力诱导透明和放大现象。Xing 等^[28]从理论上研究了复合光力系统中的四波混频响应。

基于以上的研究,本文研究了由泵浦光和探测光同时驱动的三腔复合光力系统中探测场的透射系数和四波混频现象。主要讨论了辅助腔对探测场的透射系数和四波混频谱的影响。结果发现:利用透明窗口之间的距离,可以实现两个光学腔之间耦合强度的精确测量;增大两个光学腔之间的耦合强度,可以在共振处得到较大透射率。此外,利用四波混频谱中吸收峰的位置,可以准确测量机械振子的振动频率。改变双腔之间的耦合强度和机械振子的频率,四波混频谱会有显著变化。

2 模型和理论

本文研究的复合光力系统的物理模型如图 1 所示,一个共振频率为 ω_a 的微波腔 a 和一个共振频率为 ω_{c_1} 的光学腔 c_1 共同与一个振动频率为 ω_m 的纳米机械振子 b 耦合,同时另一个共振频率为 ω_{c_2} 的光学腔 c_2 与光学腔 c_1 通过交换能量耦合^[29]。一束振幅为 $E_e [|E_e| = \sqrt{2P_e / (\hbar\Omega_e)}]$ 、频率为 Ω_e 、功率为 P_e 的强泵浦场对微波腔 a 进行驱动,其中 \hbar 为普朗克常量。一束振幅为 $E_o [|E_o| = \sqrt{2P_o / (\hbar\Omega_o)}]$ 、频率为 Ω_o 、功率为 P_o 的强泵浦场和一束振幅为 $E_p [|E_p| = \sqrt{2P_p / (\hbar\Omega_p)}]$ 、频率为 Ω_p 、功率为 P_p 的弱探测场同时对光学腔 c_1 进行驱动。整个系统的哈密顿量 ($\hbar=1$)^[14,30-32] 为

收稿日期: 2022-07-13; 修回日期: 2022-08-07; 录用日期: 2022-09-07; 网络首发日期: 2022-09-17

基金项目: 国家自然科学基金(62061028)、上海市特殊人工微结构材料与技术重点实验室开放课题基金(ammt2021A-4)、江西省杰出青年人才资助计划(20162BCB23009)

通信作者: *nculqh@163.com

$$H = \omega_a a^\dagger a + \omega_m b^\dagger b + \omega_{c_1} c_1^\dagger c_1 + \omega_{c_2} c_2^\dagger c_2 - g_e a^\dagger a (b^\dagger + b) - g_o c_1^\dagger c_1 (b^\dagger + b) + J (c_1^\dagger c_2 + c_1 c_2^\dagger) + i\sqrt{\kappa_{e,\text{ext}}/2} E_e [a^\dagger \exp(-i\Omega_e t) - a \exp(i\Omega_e t)] + i\sqrt{\kappa_{o,\text{ext}}/2} E_o [c_1^\dagger \exp(-i\Omega_o t) - c_1 \exp(i\Omega_o t)] + i\sqrt{\kappa_{o,\text{ext}}/2} E_p [c_1^\dagger \exp(-i\Omega_p t) - c_1 \exp(i\Omega_p t)], \quad (1)$$

式中: t 为时间; g_e 和 g_o 分别为纳米机械振子 b 与微波腔 a 及纳米机械振子 b 与光学腔 c_1 的耦合强度; J 为腔 c_1 与腔 c_2 之间的耦合强度; 算符 $a(a^\dagger)$ 、 $b(b^\dagger)$ 、 $c_1(c_1^\dagger)$ 、 $c_2(c_2^\dagger)$ 分别为微波腔、纳米机械振子、光学腔 c_1 和光学

腔 c_2 的湮灭算符(产生算符); $\omega_a a^\dagger a$ 、 $\omega_m b^\dagger b$ 、 $\omega_{c_1} c_1^\dagger c_1$ 和 $\omega_{c_2} c_2^\dagger c_2$ 分别为微波腔、纳米机械振子、光学腔 c_1 和光学腔 c_2 的自由哈密顿量; $\kappa_{e,\text{ext}}$ ($\kappa_{o,\text{ext}}$) 为外部耦合引起的衰减率。

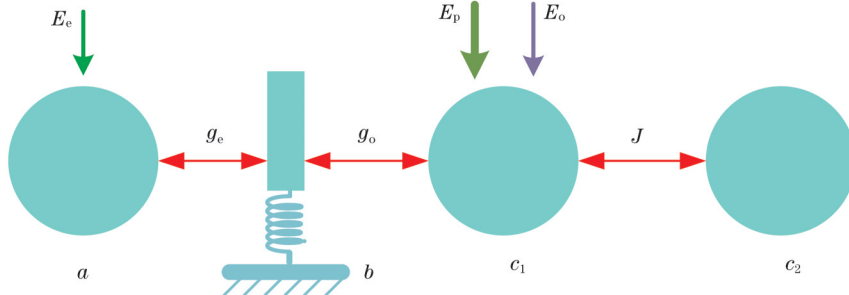


图 1 物理模型示意图
Fig. 1 Schematic of physical model

在频率为 Ω_e 和 Ω_o 的强泵浦场的旋转框架下, 复合光力系统的哈密顿量为

$$H = \Delta_a a^\dagger a + \omega_m b^\dagger b + \Delta_{c_1} c_1^\dagger c_1 + \Delta_{c_2} c_2^\dagger c_2 - g_e a^\dagger a (b^\dagger + b) - g_o c_1^\dagger c_1 (b^\dagger + b) + J (c_1^\dagger c_2 + c_1 c_2^\dagger) + i\sqrt{\kappa_{e,\text{ext}}/2} E_e (a^\dagger - a) + i\sqrt{\kappa_{o,\text{ext}}/2} E_o (c_1^\dagger - c_1) + i\sqrt{\kappa_{o,\text{ext}}/2} E_p [c_1^\dagger \exp(-i\delta t) - c_1 \exp(i\delta t)], \quad (2)$$

式中: $\Delta_a = \omega_a - \Omega_e$, $\Delta_{c_1} = \omega_{c_1} - \Omega_o$, $\Delta_{c_2} = \omega_{c_2} - \Omega_o$; δ 为探测场和泵浦场之间的失谐量, $\delta = \Omega_p - \Omega_o$

通过海森堡运动方程 $\frac{dO}{dt} = \frac{1}{i\hbar} [O, H]$ (O 为算符)

和对易关系 $[a, a^\dagger] = 1$, 得到量子朗之万方程为

$$\frac{da}{dt} = -\left(i\Delta_a + \frac{\kappa_e}{2}\right)a + ig_e a Q + \sqrt{\kappa_{e,\text{ext}}/2} E_e, \quad (3)$$

$$\frac{dc_1}{dt} = -\left(i\Delta_{c_1} + \frac{\kappa_o}{2}\right)c_1 + ig_o c_1 Q - iJc_2 + \sqrt{\kappa_{o,\text{ext}}/2} [E_o + E_p \exp(i\delta t)], \quad (4)$$

$$\frac{dc_2}{dt} = -\left(i\Delta_{c_2} + \frac{\kappa_t}{2}\right)c_2 - iJc_1, \quad (5)$$

$$\frac{d^2Q}{dt^2} + \gamma_m \frac{dQ}{dt} + \omega_m^2 Q = 2\omega_m g_e a^\dagger a + 2\omega_m g_o c_1^\dagger c_1, \quad (6)$$

式中: $Q = b^\dagger + b$; $\kappa_e(\kappa_o)$ 为微波腔 a (光学腔 c_1) 的衰减率; γ_m 为机械振子 b 的衰减率; κ_t 为光学腔 c_2 的衰减率。

为了求解式(3)~(6), 进行近似代换, 即

$$a(t) = a_0 + a_+ \exp(-i\delta t) + a_- \exp(i\delta t), \quad (7)$$

$$Q(t) = Q_0 + Q_+ \exp(-i\delta t) + Q_- \exp(i\delta t), \quad (8)$$

$$c_1(t) = c_{10} + c_{1+} \exp(-i\delta t) + c_{1-} \exp(i\delta t), \quad (9)$$

$$c_2(t) = c_{20} + c_{2+} \exp(-i\delta t) + c_{2-} \exp(i\delta t), \quad (10)$$

式中: a_0 为腔 a 在稳态时的振幅; a_+ 、 a_- 为系数; Q_0 为稳态时的机械位移; Q_+ 、 Q_- 为系数; c_{10} 为腔 c_1 在稳态时的振幅; c_{1+} 、 c_{1-} 为系数; c_{20} 为腔 c_2 在稳态时的振幅; c_{2+} 、 c_{2-} 为系数。

忽略高阶非线性项, 得到稳态值为

$$a_0 = \frac{\sqrt{\kappa_{e,\text{ext}}/2} E_e}{\left(i\Delta_a + \frac{\kappa_e}{2}\right) - ig_e Q_0}, \quad (11)$$

$$Q_0 = \frac{2g_e n_a + 2g_o n_{c_1}}{\omega_m}, \quad (12)$$

$$c_{10} = \frac{\sqrt{\kappa_{o,\text{ext}}/2} E_o}{\left(i\Delta_{c_1} + \frac{\kappa_o}{2}\right) - ig_o Q_0 + iJ a_0}, \quad (13)$$

$$c_{20} = \frac{-iJ c_1}{i\Delta_{c_2} + \frac{\kappa_t}{2}}, \quad (14)$$

式中: n_a 为腔 a 内的光子数; n_{c_1} 为腔 c_1 内的光子数; $\alpha = \frac{-iJ}{i\Delta_{c_2} + \frac{\kappa_t}{2}}$ 。式(11)~(14)决定了腔内光子数 ($n_a = |a_0|^2$, $n_{c_1} = |c_{10}|^2$), 即

$$n_a = \frac{\kappa_{e,\text{ext}}/2 E_e^2}{\kappa_e^2/4 + \left[\Delta_a - \frac{2g_e}{\omega_m} (g_e n_a + g_o n_{c_1}) \right]^2}, \quad (15)$$

$$n_{c_1} = \frac{E_o^2 \kappa_o/2}{\frac{\kappa_o^2}{4} + \left[-\Delta_{c_1} + \frac{J^2 \Delta_{c_2}}{\Delta_{c_2}^2 + \frac{\kappa_t^2}{4}} + \frac{g_o}{\omega_m} (2g_e n_a + 2g_o n_{c_1}) \right]^2 - \left(\frac{J^2 \Delta_{c_2}}{\Delta_{c_2}^2 + \frac{\kappa_t^2}{4}} \right)^2 + \frac{J^4 + J^2 \kappa_t \kappa_o/2}{\Delta_{c_2}^2 + \frac{\kappa_t^2}{4}}} \circ \quad (16)$$

此外, 通过求解式(3)~(6), 还可以得到

$$c_{1-} = \frac{\sqrt{\kappa_{o,\text{ext}}/2} i\Phi_3^* \frac{\kappa_{o,\text{ext}}}{2} E_p E_o^2 g_o^2}{\Phi_6^* \Phi_8^* \Phi_7^* \Phi_8^* \left(1 - \frac{i\Phi_3^* g_e^2 n_a}{\Phi_5^*} + \Phi \frac{i\Phi_3^* g_e^2 n_a}{\Phi_4^*} - \frac{i\Phi_3^* g_o^2 n_{c_1}}{\Phi_7^*} + \frac{i\Phi_3^* g_o^2 n_{c_1}}{\Phi_6^*} \right)}, \quad (17)$$

$$c_{1+} = \frac{\sqrt{\kappa_{o,\text{ext}}/2} E_p}{-i\delta + \left(i\Delta_{c_1} + \frac{\kappa_o}{2} \right) - ig_o Q_0 + iJ\Phi_1} + \frac{ig_o}{-i\delta + \left(i\Delta_{c_1} + \frac{\kappa_o}{2} \right) - ig_o Q_0 + iJ\Phi_1} \times \frac{\sqrt{\kappa_{o,\text{ext}}/2} \Phi_3 g_o \frac{\kappa_{o,\text{ext}}}{2} E_p E_o^2}{\Phi_6^* \Phi_8^* \Phi_8 \left(1 - \frac{i\Phi_3^* g_e^2 n_a}{\Phi_4^*} + \frac{i\Phi_3^* g_e^2 n_a}{\Phi_5^*} - \frac{i\Phi_3^* g_o^2 n_{c_1}}{\Phi_6^*} + \frac{i\Phi_3^* g_o^2 n_{c_1}}{\Phi_7^*} \right)}, \quad (18)$$

式中: $\Phi_1 = \frac{-iJ}{-i\delta + \left(i\Delta_{c_2} + \frac{\kappa_t}{2} \right)}$; $\Phi_2 = \frac{-iJ}{i\delta + \left(i\Delta_{c_2} + \frac{\kappa_t}{2} \right)}$; $\Phi_3 = \frac{2\omega_m}{-\delta^2 - i\delta\gamma_m + \omega_m^2}$; $\Phi_4 = -i\delta - ig_e Q_0 + \left(i\Delta_a + \frac{\kappa_e}{2} \right)$; $\Phi_5 = -i\delta + ig_e Q_0 + \left(-i\Delta_a + \frac{\kappa_e}{2} \right)$; $\Phi_6 = -i\delta + \left(i\Delta_{c_1} + \frac{\kappa_o}{2} \right) - ig_o Q_0 + iJ\Phi_1$; $\Phi_7 = -i\delta + \left(-i\Delta_{c_1} + \frac{\kappa_o}{2} \right) + ig_o Q_0 - iJ\Phi_2^*$; $\Phi_8 = \left(-i\Delta_{c_1} + \frac{\kappa_o}{2} \right) + ig_o Q_0 - iJ\alpha^*$; * 表示取共轭。

引入标准的输入-输出理论^[2]得到

$$c_{\text{out}}(t) = \left(E_o - \sqrt{\kappa_{o,\text{ext}}/2} c_{1-} \right) \exp(-i\Omega_o t) + \left(E_p - \sqrt{\kappa_{o,\text{ext}}/2} c_{1+} \right) \exp[-i(\delta + \Omega_o)t] - \sqrt{\kappa_{o,\text{ext}}/2} c_{1-} \times \exp[-i(\delta - \Omega_o)t] = \left(E_o - \sqrt{\kappa_{o,\text{ext}}/2} c_{1-} \right) \exp(-i\Omega_o t) + \left(E_p - \sqrt{\kappa_{o,\text{ext}}/2} c_{1+} \right) \exp(-i\Omega_p t) - \sqrt{\kappa_{o,\text{ext}}/2} c_{1-} \exp[-i(2\Omega_o - \Omega_p)t], \quad (19)$$

式中: $c_{\text{out}}(t)$ 为输出场算符; 第一项是振幅为 E_o 、频率为 Ω_o 的驱动场; 第二项是振幅为 E_p 、频率为 Ω_p 的探测场; 最后一项是频率为 $2\Omega_o - \Omega_p$ 的四波混频场。四波混频场的强度^[16]定义为

$$F_{\text{FWM}} = \left| \frac{\sqrt{\kappa_{o,\text{ext}}/2} c_{1-}}{E_p} \right|^2 = \left| \frac{i\Phi_3^* \frac{\kappa_{o,\text{ext}}^2}{4} E_o^2 g_o^2}{\Phi_6^* \Phi_8^* \Phi_7^* \Phi_8^* \left(1 - \frac{i\Phi_3^* g_e^2 n_a}{\Phi_5^*} + \frac{i\Phi_3^* g_e^2 n_a}{\Phi_4^*} - \frac{i\Phi_3^* g_o^2 n_{c_1}}{\Phi_7^*} + \frac{i\Phi_3^* g_o^2 n_{c_1}}{\Phi_6^*} \right)} \right|^2 \circ \quad (20)$$

探测场的透射系数 $t(\Omega_p)$ 为输出场与输入场的振幅之比, 即

$$t(\Omega_p) = \frac{E_p - \sqrt{\kappa_{o, ext}/2} c_{1+}}{E_p} = 1 - \frac{\kappa_{o, ext}/2}{-i\delta + \left(i\Delta_{c_1} + \frac{\kappa_o}{2}\right) - ig_o Q_0 + iJ\Phi_1} - \frac{ig_o}{-i\delta + \left(i\Delta_{c_1} + \frac{\kappa_o}{2}\right) - ig_o Q_0 + iJ\Phi_1} \times \\ \frac{\Phi_3 g_o \frac{\kappa_{o, ext}}{4} E_o^2}{\Phi_6 \Phi_8^* \Phi_8 \left(1 - \frac{i\Phi_3 g_e^2 n_a}{\Phi_4} + \frac{i\Phi_3 g_e^2 n_a}{\Phi_5} - \frac{i\Phi_3 g_o^2 n_{c_1}}{\Phi_6} + \frac{i\Phi_3 g_o^2 n_{c_1}}{\Phi_7}\right)} \quad (21)$$

利用以上结果讨论双腔之间的耦合系数和机械振子的频率对三腔复合光力系统中探测场的透射系数和四波混频现象的影响。

3 数值结果与讨论

为了更好地研究系统的光学响应,选择实验上可实现的参数^[33-35]: $\kappa_o = 2\pi \times 1.65 \text{ MHz}$, $\kappa_e = 2\pi \times 1.6 \text{ MHz}$, $\kappa_{o, ext} = 0.11\kappa_e$, $\kappa_{o, ext} = 0.76\kappa_o$, $J = \kappa_o$, $g_o = 2\pi \times 27 \text{ Hz}$, $g_e = 2\pi \times 2.7 \text{ Hz}$, $\omega_a = 2\pi \times 7.1 \text{ GHz}$, $\omega_m = 2\pi \times 5.6 \text{ MHz}$, $\omega_{c_1} = \omega_{c_2} = 2\pi \times 282 \text{ THz}$, $\gamma_m = 2\pi \times 4 \text{ Hz}$ 。

在两束泵浦激光的作用下,复合系统的光学响应可以通过探测场的透射谱来表征。当 $\Delta_{c_1} = \Delta_{c_2} = -\omega_m$, $\Delta_a = \omega_m$ 时,光学腔 c_1 和 c_2 被驱动至蓝边带,此时微波腔 a 被驱动至红边带。当光学腔 c_1 和 c_2 的耦合强度

$J = 0, 0.5\kappa_o, \kappa_o, 2\kappa_o$ 时探测场的透射谱随探测场-腔场的失谐量 $\Delta_p = \Omega_p - \omega_{c_1}$ 的变化曲线如图 2 所示。当 $J = 0$ 时,如图 2 中实线所示,系统中没有光学腔 c_2 的作用,探测场透射谱呈现洛伦兹线型。但是当两个光学腔之间的耦合强度打开时,即 $J = 0.5\kappa_o, \kappa_o, 2\kappa_o$ 时,位于 $\Delta_p = 0$ 处的洛伦兹峰分裂为两个对称的峰和一个透明窗口^[36-37]。从图 2 还可以明显看出,随着耦合强度 J 的增大,峰间距逐渐增大。共振处 ($\Delta_p = 0$) 探测场的透射率随着 J 的增大而增大。图 3 为峰间距和共振处透射率随耦合强度 J 的变化情况。可以发现,峰间距与耦合强度 J 呈线性关系。此外,当耦合强度 J 增大到某个值时,共振处透射率的增大趋势逐渐缓慢。

接下来讨论该复合系统中的四波混频现象。图 4 绘制了耦合强度 $J = 0, 0.5\kappa_o, \kappa_o, 2\kappa_o$ 时四波混频强度随

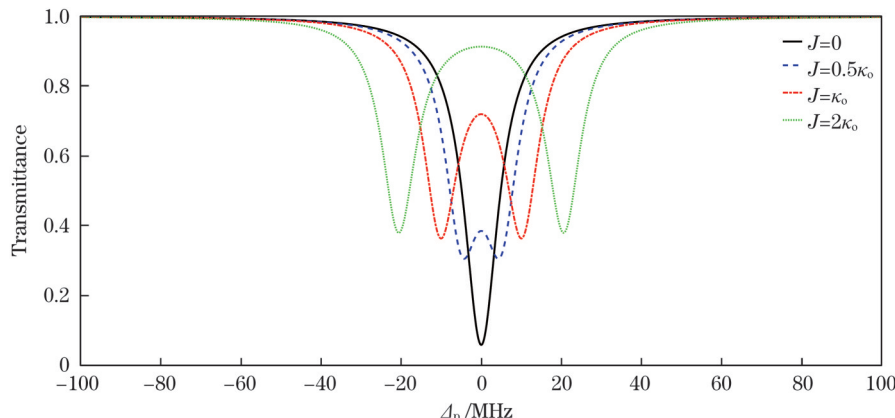


图 2 $J = 0, 0.5\kappa_o, \kappa_o, 2\kappa_o$ 时探测场的透射谱随失谐量 $\Delta_p = \Omega_p - \omega_{c_1}$ 的变化

Fig. 2 Transmission spectrum of probe field versus $\Delta_p = \Omega_p - \omega_{c_1}$ when $J = 0, 0.5\kappa_o, \kappa_o, 2\kappa_o$

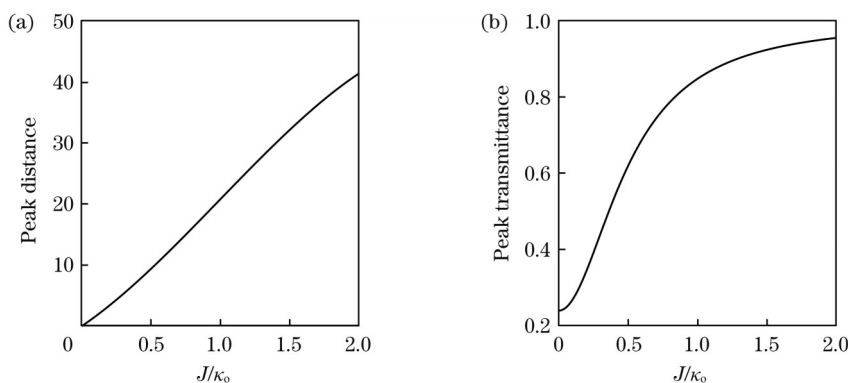


图 3 耦合强度 J 对探测场透射谱的影响。(a) 峰间距; (b) $\Delta_p = 0$ 处的峰值透射率

Fig. 3 Influence of coupling strength J on transmission spectrum of probe field. (a) Peak distance; (b) peak transmittance at $\Delta_p = 0$

探测场-腔场失谐量 Δ_p 的变化情况。机械振子 b 的频率保持在 $\omega_m = 2\pi \times 5.6$ MHz 不变, 在共振的情况下, 即 $\Delta_{c_1} = \Delta_{c_2} = \Delta_a = 0$ 时, 从图 4(a) 可以看出, 当 $J = 0$ 时, 四波混频谱有三个峰, 一个是 $\Delta_p = 0$ 处的洛伦兹峰, 两个是 $\Delta_p = 0$ 两侧的分裂峰。两个分裂峰的出现可以用单腔光力系统中的缀饰态理论来解释^[38]。当系统中加

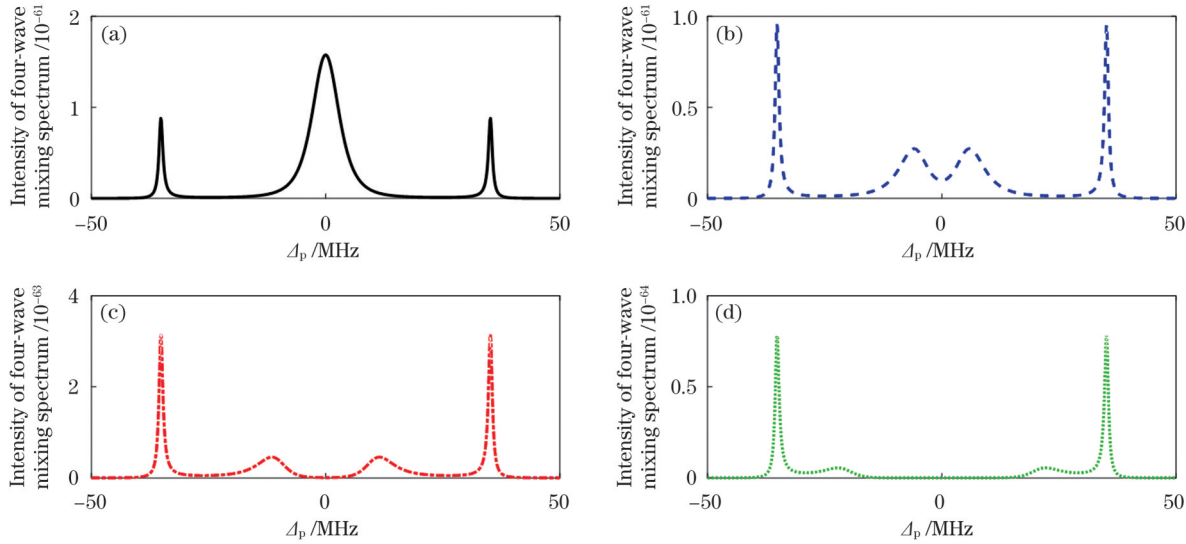


图 4 不同 J 下四波混频谱强度随探测场-腔场失谐量 Δ_p 的变化。(a) $J = 0$; (b) $J = 0.5\kappa_o$; (c) $J = \kappa_o$; (d) $J = 2\kappa_o$

Fig. 4 Intensity of four-wave mixing spectrum versus Δ_p under different J . (a) $J = 0$; (b) $J = 0.5\kappa_o$; (c) $J = \kappa_o$; (d) $J = 2\kappa_o$

基于图 4 所示的研究情况, 接下来讨论当复合系统中没有辅助腔 c_2 , 改变机械振子 b 的频率, 如 $\omega_m = 2\pi \times 4.6$ MHz, $\omega_m = 2\pi \times 5.6$ MHz, $\omega_m = 2\pi \times 6.6$ MHz 时, 四波混频谱随探测场-腔场失谐量 Δ_p 的变化情况, 结果如图 5 所示。可以看出, 当机械振子 b 的频率 ω_m 逐渐增大时, 四波混频谱峰值逐渐减小。同时, 可以观察到四波混频谱位于中间洛伦兹峰两侧的尖峰正处于 $\Delta_p = \pm \omega_m$ 位置处, 表明尖峰的位置正好对应机械振子 b 的频率。这种现象的物理本质是机械振动模式与两束光场相互作用而产生了量子相干效应^[19,40]。图 5 表明, 通过双场探测手段可以实现机械振子振动频率的

入辅助腔 c_2 后, 从图 4(b)~(d) 可以发现, 四波混频谱发生了显著变化, 出现了双色光力诱导透明现象。图 4(a) 中的洛伦兹峰分裂为两个峰, 且随着耦合强度 J 的增大, 这两个峰的峰值逐渐减小, 峰间距逐渐增大。这种现象可以用超模理论^[39]来解释。原本两侧尖峰的位置不变但峰值逐渐减小。

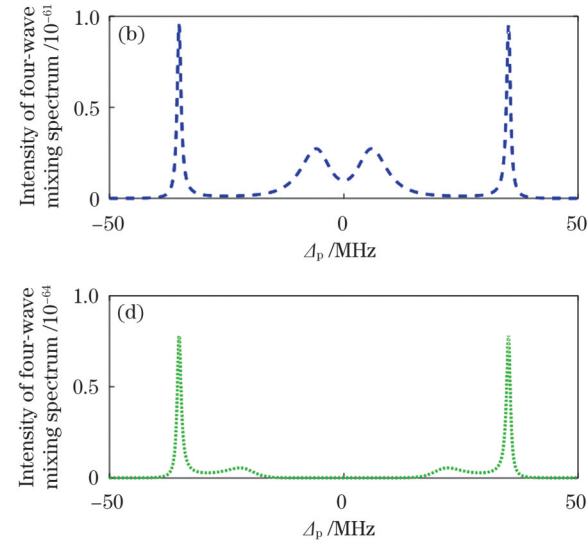


图 5 $J = 0$ 时不同机械振子频率下四波混频谱强度随 $\Delta_p/2\pi$ 的变化

Fig. 5 Intensity of four-wave mixing spectrum versus $\Delta_p/2\pi$ under different mechanical resonator frequencies when $J = 0$

精确测量。首先使泵浦场频率与光学腔场频率相等 ($\Delta_p = 0$), 然后利用探测场扫描复合系统, 此时四波混频谱中尖峰的位置恰好对应机械振子的频率。

如图 6 所示, 进一步绘制复合系统中加入辅助腔 c_2 ($J = \kappa_o$), 并且机械振子 b 的频率分别为 $\omega_m = 2\pi \times 4.6$ MHz, $\omega_m = 2\pi \times 5.6$ MHz, $\omega_m = 2\pi \times 6.6$ MHz 时, 四波混频谱随探测场-腔场失谐量 Δ_p 的变化。随着机械振子频率的增大, 中间两个对称的分裂峰强度和峰间距均减小, 且两侧尖峰的位置正好对应机械振子的三种不同频率。图 6 结果表明, 改变机械振子的频率会使四波混频谱强度发生变化。

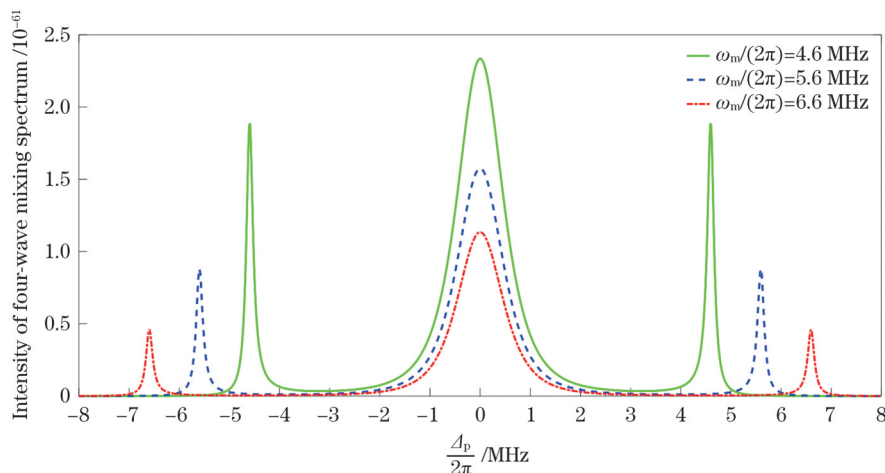


图 5 $J = 0$ 时不同机械振子频率下四波混频谱强度随 $\Delta_p/2\pi$ 的变化

Fig. 5 Intensity of four-wave mixing spectrum versus Δ_p when $J = 0$

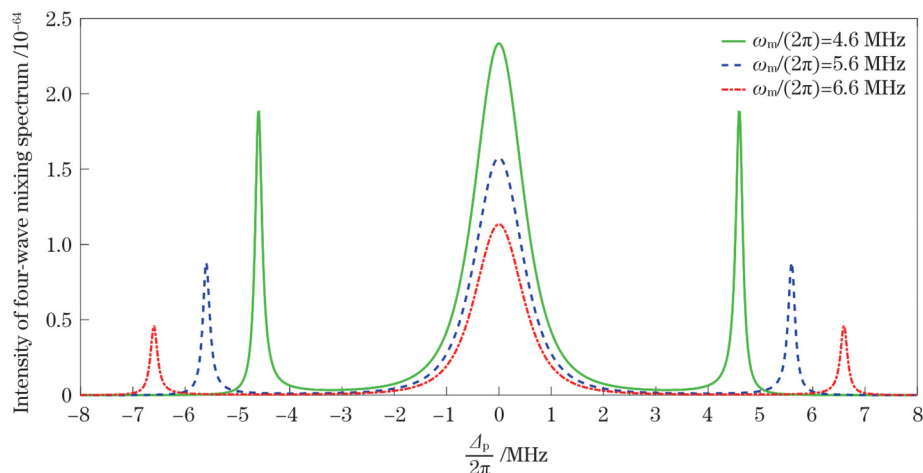


图 6 $J=\kappa_o$ 时不同机械振子频率下四波混频谱强度随 $\Delta_p/2\pi$ 的变化

Fig. 6 Intensity of four-wave mixing spectrum versus $\Delta_p/2\pi$ under different mechanical resonator frequencies when $J=\kappa_o$

4 结 论

研究了由两个光学腔和一个微波腔以及一个机械振子组成的复合光力系统中的光力诱导透明现象和四波混频现象。当微波腔被驱动到红边带而两个光学腔被驱动到蓝边带时, 改变两个光学腔之间的耦合强度, 光力诱导透明现象发生变化。此外, 讨论了在共振的情况下, 通过控制两个光学腔之间的耦合强度和改变机械振子的频率, 可以对四波混频谱进行调制。同时, 还提出了一种测量机械振子频率的非线性光学方法, 即四波混频谱中两侧尖峰的位置正好对应机械振子的频率。

参 考 文 献

- [1] Aspelmeyer M, Meystre P, Schwab K. Quantum optomechanics [J]. Physics Today, 2012, 65(7): 29-35.
- [2] Aspelmeyer M, Kippenberg T J, Marquardt F. Cavity optomechanics[J]. Reviews of Modern Physics, 2014, 86(4): 1391-1452.
- [3] Kippenberg T J, Vahala K J. Cavity optomechanics: back-action at the mesoscale[J]. Science, 2008, 321(5893): 1172-1176.
- [4] Marquardt F, Girvin S M. Optomechanics[J]. Physics, 2009, 2: 40.
- [5] Liu Y C, Hu Y W, Huang Z W, et al. Review of cavity optomechanical cooling[J]. Chinese Physics B, 2013, 22(11): 105-117.
- [6] Grudinin I S, Lee H, Painter O, et al. Phonon laser action in a tunable, two-level system[J]. Physical Review Letters, 2010, 104(8): 083901.
- [7] Li J J, Zhu K D. All-optical mass sensing with coupled mechanical resonator systems[J]. Physics Reports, 2013, 525(3): 223-254.
- [8] Wollman E E, Lei C U, Weinstein A J, et al. Quantum squeezing of motion in a mechanical resonator[J]. Science, 2015, 349(6251): 952-955.
- [9] Brooks D W C, Botter T, Schreppler S, et al. Non-classical light generated by quantum-noise-driven cavity optomechanics[J]. Nature, 2012, 488(7412): 476-480.
- [10] Tian L. Robust photon entanglement via quantum interference in optomechanical interfaces[J]. Physical Review Letters, 2013, 110(23): 233602.
- [11] Massel F, Heikkilä T T, Pirkkalainen J M, et al. Microwave amplification with nanomechanical resonators[J]. Nature, 2011, 480(7377): 351-354.
- [12] Chan J, Alegre T P M, Safavi-Naeini A H, et al. Laser cooling of a nanomechanical oscillator into its quantum ground state[J]. Nature, 2011, 478(7367): 89-92.
- [13] Wang Y D, Clerk A A. Using interference for high fidelity quantum state transfer in optomechanics[J]. Physical Review Letters, 2012, 108(15): 153603.
- [14] Weis S, Rivière R, Deléglise S, et al. Optomechanically induced transparency[J]. Science, 2010, 330(6010): 1520-1523.
- [15] Liao Q H, Xiao X, Nie W J, et al. Transparency and tunable slow-fast light in a hybrid cavity optomechanical system[J]. Optics Express, 2020, 28(4): 5288-5305.
- [16] Li J H, Yu R, Ding C L, et al. Optical bistability and four-wave mixing with a single nitrogen-vacancy center coupled to a photonic crystal nanocavity in the weak-coupling regime[J]. Optics Express, 2014, 22(12): 15024-15038.
- [17] Huang S M, Agarwal G S. Normal-mode splitting and antibunching in Stokes and anti-Stokes processes in cavity optomechanics: radiation-pressure-induced four-wave-mixing cavity optomechanics[J]. Physical Review A, 2010, 81(3): 033830.
- [18] Jia W Z, Wei L F, Li Y, et al. Phase-dependent optical response properties in an optomechanical system by coherently driving the mechanical resonator[J]. Physical Review A, 2015, 91(4): 043843.
- [19] Jiang C, Cui Y S, Liu H X. Controllable four-wave mixing based on mechanical vibration in two-mode optomechanical systems[J]. EPL (Europhysics Letters), 2013, 104(3): 34004.
- [20] Xiao X, Liao Q H, Zhou N R, et al. Tunable optical second-order sideband effects in a parity-time symmetric optomechanical system [J]. Science China Physics, Mechanics & Astronomy, 2020, 63(11): 114211.
- [21] Wang J. Ground-state cooling based on a three-cavity optomechanical system in the unresolved-sideband regime[J]. Chinese Physics B, 2021, 30(2): 024204.
- [22] Jiang C, Ji B W, Cui Y S, et al. Quantum-limited directional amplifier based on a triple-cavity optomechanical system[J]. Optics Express, 2018, 26(12): 15255-15267.
- [23] Chen H J, Wu H W, Yang J Y, et al. Controllable optical bistability and four-wave mixing in a photonic-molecule optomechanics[J]. Nanoscale Research Letters, 2019, 14(1): 73.
- [24] 喻富, 肖添, 何高倩, 等. 超导量子比特耦合微波腔和机械谐振器系统的探测场吸收特性研究[J]. 激光与光电子学进展, 2022, 59(3): 0327001.
- Yu F, Xiao T, He G Q, et al. Probe absorption properties of a superconducting qubit coupled to microwave cavity and mechanical resonator[J]. Laser & Optoelectronics Progress, 2022, 59(3):

- 0327001.
- [25] 陈咏雷, 陈华俊, 刘云鹤, 等. 基于复合旋转光力系统中非线性光学特性研究[J]. 光学学报, 2023, 43(1): 0119001.
Chen Y L, Chen H J, Liu Y H, et al. Nonlinear behavior research based on hybrid spinning optomechanical system[J]. Acta Optica Sinica, 2023, 43(1): 0119001.
- [26] 陈冬成, 周岳辉, 黄金凤, 等. 混合腔光力系统的双光子散射[J]. 光学学报, 2022, 42(3): 0327015.
Chen D C, Zhou Y H, Huang J F, et al. Two-photon scattering in mixed cavity optomechanical system[J]. Acta Optica Sinica, 2022, 42(3): 0327015.
- [27] 王婧, 田雪冬. 基于非旋转波近似效应的完美光力诱导透明和放大[J]. 激光与光电子学进展, 2021, 58(5): 0512002.
Wang J, Tian X D. Ideal optomechanically induced transparency and amplification based on nonrotating wave approximation effect [J]. Laser & Optoelectronics Progress, 2021, 58(5): 0512002.
- [28] Xing H W, Chen B, Xing L L, et al. Controllable four-wave mixing based on quantum dot-cavity coupling system[J]. Communications in Theoretical Physics, 2021, 73(5): 055101.
- [29] Liao J Q, Wu Q Q, Nori F. Entangling two macroscopic mechanical mirrors in a two-cavity optomechanical system[J]. Physical Review A, 2014, 89(1): 014302.
- [30] Chen H J, Hou B C, Yang J Y. Controllable coherent optical response in a ring cavity optomechanical system[J]. Physica E: Low-Dimensional Systems and Nanostructures, 2021, 125: 114394.
- [31] Barzanjeh S, Abdi M, Milburn G J, et al. Reversible optical-to-microwave quantum interface[J]. Physical Review Letters, 2012, 109(13): 130503.
- [32] Jiang C, Cui Y S, Liu H X, et al. Controllable optical response in hybrid opto-electromechanical systems[J]. Chinese Physics B, 2015, 24(5): 054206.
- [33] Teufel J D, Donner T, Li D L, et al. Sideband cooling of micromechanical motion to the quantum ground state[J]. Nature, 2011, 475(7356): 359-363.
- [34] Teufel J D, Li D L, Allman M S, et al. Circuit cavity electromechanics in the strong-coupling regime[J]. Nature, 2011, 471(7337): 204-208.
- [35] Andrews R W, Peterson R W, Purdy T P, et al. Bidirectional and efficient conversion between microwave and optical light[J]. Nature Physics, 2014, 10(4): 321-326.
- [36] 贺庆. 混合腔光力系统诱导透明及其相关现象的研究[D]. 武汉: 华中科技大学, 2019: 31-45.
He Q. Studies on induced transparency and related phenomena in hybrid cavity optomechanical systems[D]. Wuhan: Huazhong University of Science and Technology, 2019: 31-45.
- [37] Zhu Y J, Bai C H, Wang T, et al. Optomechanically induced transparency, amplification, and fast-slow light transitions in an optomechanical system with multiple mechanical driving phases[J]. Journal of the Optical Society of America B, 2020, 37(3): 888-893.
- [38] Jiang C, Chen B, Li J J, et al. Mass sensing based on a circuit cavity electromechanical system[J]. Journal of Applied Physics, 2011, 110(8): 083107.
- [39] Zhang X Y, Zhou Y H, Guo Y Q, et al. Optomechanically induced transparency in optomechanics with both linear and quadratic coupling[J]. Physical Review A, 2018, 98(5): 053802.
- [40] 陈华俊. 基于石墨烯光力系统的非线性光学效应及非线性光学质量传感[J]. 物理学报, 2020, 69(13): 134203.
Chen H J. Nonlinear optical effect and nonlinear optical mass sensor based on graphene optomechanical system[J]. Acta Physica Sinica, 2020, 69(13): 134203.

Transmission Spectrum and Four-Wave Mixing in Three-Cavity Hybrid Optomechanical System

Liao Qinghong*, Qiu Haiyan, Yu Fu, Xiao Min

Department of Electronic Information Engineering, Nanchang University, Nanchang 330031, Jiangxi, China

Abstract

Objective The rapid development of cavity optomechanical systems has attracted extensive attention, and these systems are widely used in quantum information and precision measurement. In recent years, three-cavity optomechanical systems have attracted considerable attention. Compared with the single-mode optomechanical system, the multiple-mode system provides significantly higher flexible controllability. Furthermore, optomechanically induced transparency and four-wave mixing have been research hotspots in different optomechanical systems. For example, the four-wave mixing in a hybrid optomechanical system is theoretically investigated, which has important implications for the nonlinear optical properties. It is of great significance for theoretically exploring the transmission spectrum and four-wave mixing in a three-cavity optomechanical system.

Methods The hybrid optomechanical system consists of a microwave cavity a with resonance frequency ω_a and an optical cavity c_1 with resonance frequency ω_{c_1} , which are coupled to a common mechanical resonator b , while an optical cavity c_2 with resonance frequency ω_{c_2} is coupled to the optical cavity c_1 . A strong pump laser beam E_e with frequency Ω_e is applied to the microwave cavity a . A weak probe laser beam E_p with frequency Ω_p and a strong pump laser beam E_o with frequency Ω_o are applied to the optical cavity c_1 simultaneously. In the rotating frame of the pump fields with frequency Ω_e and Ω_o , the whole Hamiltonian of the system is obtained. According to the Heisenberg equation and making the ansatz, we finally obtain the transmission spectrum and the four-wave mixing spectrum intensity. Then, we investigate how the evolutions of the transmission spectrum and the four-wave mixing spectrum are affected by the coupling strength and the frequency of the mechanical resonator.

Results and Discussions When the optical cavity c_2 is absent in the hybrid optomechanical system ($J=0$), the transmission spectrum of the probe field shows a Lorentzian line shape. However, when $J \neq 0$, the Lorentzian peak splits into two symmetrical peaks and a transparent window occurs (Fig. 2). It is clear that with the increase in the coupling strength from $J=0.5\kappa_o$ to $J=2\kappa_o$, the

distance between the peaks increases, and the peak value of the transmission spectrum of the probe field also increases (Fig. 3). We depict the variation of the four-wave mixing spectrum with the detuning of the probe field-cavity field Δ_p for $J=0, 0.5\kappa_o, \kappa_o, 2\kappa_o$ when $\omega_m=2\pi\times 5.6$ MHz. In the case of $\Delta_{c_1}=\Delta_{c_2}=\Delta_a=0$, when $J=0$, the four-wave mixing spectrum has three peaks. A Lorentzian peak locates at $\Delta_p=0$ and two splitting peaks locate on both sides of the Lorentzian peak [Fig. 4(a)]. With the choice of $J\neq 0$, a significant change in the four-wave mixing spectrum can be observed. The Lorentzian peak splits into two peaks. As the coupling strength J increases, the peak value decreases greatly and the distance between the peaks gradually increases [Figs. 4(b)–(d)]. Next, we study how the evolution of the four-wave mixing spectrum is affected by the frequency of the mechanical resonator while the optical cavity c_2 is not in the hybrid optomechanical system ($J=0$). It can be seen that as the frequency of the mechanical resonator increases, the peak value of the four-wave mixing spectrum gradually decreases. Further, the peaks on both sides of the four-wave mixing spectrum located at $\pm\Delta_p$ just correspond to the frequency ω_m of the mechanical resonator (Fig. 5). Moreover, we investigate the four wave mixing spectrum as a function of the detuning Δ_p for the frequencies of mechanical resonator of $\omega_m=2\pi\times 4.6$ MHz, $\omega_m=2\pi\times 5.6$ MHz, and $\omega_m=2\pi\times 6.6$ MHz when $J=\kappa_o$. As the frequency of the mechanical resonator increases, the peak value and the distance between the two symmetrical splitting peaks in the middle decrease. The positions of the peaks on both sides exactly correspond to the three different frequencies of the mechanical resonator. The results show that the four-wave mixing can be tuned by the frequency of the mechanical resonator (Fig. 6).

Conclusions We investigate the optomechanically induced transparency and four-wave mixing in a hybrid optomechanical system composed of two optical cavities, a microwave cavity, and a mechanical resonator. When the microwave cavity is driven to the red sideband and the two optical cavities are driven to the blue sideband, the optomechanically induced transparency can be changed by changing the coupling strength between the two optical cavities. Furthermore, the four-wave mixing spectrum can be modulated by controlling the coupling strength between the two optical cavities and by changing the frequency of the mechanical resonator during resonant detuning $\Delta_p=0$. At the same time, a nonlinear optical method for measuring the frequency of a mechanical resonator is provided. The positions of the peaks on both sides of the four-wave mixing spectrum correspond exactly to the frequency of the mechanical resonator. These results have important significance and application prospects in quantum sensing and quantum information processing.

Key words quantum optics; hybrid optomechanical system; transmission spectrum; four-wave mixing; optomechanically induced transparency